The role of lattice dynamics in ferroelectric switching

Qiwu Shi (shiqiwu@scu.edu.cn)
Sichuan University

Eric Parsonnet
University of California, Berkeley https://orcid.org/0000-0003-0723-6887

Xiaoxing Chen
Penn State University, University Park

Ren-Ci Peng
Xi'an Jiaotong University

Abel Fernandez
University of California, Berkeley

Natalya Fedorova
Luxembourg Institute of Science and Technology

Alexander Qualls
University of California, Berkeley https://orcid.org/0000-0001-9070-026X

Xiaoxi Huang
University of California, Berkeley

Xue Chang
Sichuan University

Hongrui Zhang
University of California, Berkeley

David Pesquera
Catalan Institute of Nanoscience and Nanotechnology https://orcid.org/0000-0003-0681-3371

Sujit Das
University of California https://orcid.org/0000-0001-9823-0207

Dmitri Nikonov
Intel Inc https://orcid.org/0000-0002-1436-1267

Ian Young
Intel Inc https://orcid.org/0000-0002-4017-5265

Long-Qing Chen
Pennsylvania State University https://orcid.org/0000-0003-3359-3781

Lane Martin
University of California, Berkeley https://orcid.org/0000-0003-1889-2513

Yen-Lin Huang

UC Berkeley

Jorge Íñiguez

Luxembourg Institute of Science and Technology

Ramamoorthy Ramesh

University of California, Berkeley https://orcid.org/0000-0003-0524-1332

Article

Keywords: lattice dynamics, ferroelectric switching, freestanding BiFeO3 membranes, substrate clamping

Posted Date: August 13th, 2021

DOI: https://doi.org/10.21203/rs.3.rs-778321/v1

Version of Record: A version of this preprint was published at Nature Communications on March 2nd, 2022. See the published version at https://doi.org/10.1038/s41467-022-28622-z.

The role of lattice dynamics in ferroelectric switching

Qiwu Shi[1,2a,*], Eric Parsonnet[3a], Xiaoxing Cheng[4a], Ren-Ci Peng[5], Abel Fernandez[1], Natalya Fedorova[6], Alexander Qualls[3], Xiaoxi Huang[1], Xue Chang[2], Hongrui Zhang[1], David Pesquera[1], Sujit Das[1], Dmitri Nikonov[7], Ian Young[7], Long-Qing Chen[4], Lane W. Martin[1,9], Yen-Lin Huang[1*], Jorge Íñiguez[6,8] and Ramamoorthy Ramesh[1,3,9*]

[1] Department of Materials Science and Engineering, University of California, Berkeley, CA 94720, USA

[2] College of Materials Science and Engineering, Sichuan University, Chengdu 610065, China

[3] Department of Physics, University of California, Berkeley, CA 94720, USA

[4] Department of Materials Science and Engineering, Penn State University, University Park, Pennsylvania 16802, USA

[5] Electronic Materials Research Laboratory, Key Laboratory of the Ministry of Education & International Center for Dielectric Research, School of Electronic Information and Engineering, Xi'an Jiaotong University, 710049 Xi'an, China

[6] Materials Research and Technology Department, Luxembourg Institute of Science and Technology, L-4362 Esch/Alzette, Luxembourg

[7] Components Research, Intel Corporation, Hillsboro, Oregon 97142, USA

[8] Department of Physics and Materials Science, University of Luxembourg, L-4422 Belvaux, Luxembourg

[9] Materials Sciences Division, Lawrence Berkeley National Laboratory, Berkeley, CA 94720, USA

[a] These authors contributed equally

Abstract:

Reducing the switching energy of ferroelectric thin films remains an important goal in the pursuit of ultralow power ferroelectric memories and magnetoelectric

spin-orbit logic devices. Here, we elucidate the fundamental role of lattice dynamics in ferroelectric switching by combining thermodynamic calculations, experiments, and phase-field simulations on both freestanding $BiFeO_3$ membranes and films clamped to a substrate. We observe a distinct evolution of the ferroelectric domain pattern, from striped, 71° ferroelastic domains (spacing of ~100 nm) in clamped $BiFeO_3$ films, to large (10's of micrometers) 180° domains or even single domain structures, in freestanding films. Through the use of piezoresponse force microscopy, X-ray diffraction, polarization-electric field hysteresis loops, and high-speed pulsed ferroelectric switching experiments, it is found that removing the constraints imposed by the requirement of macroscopic continuity of deformation (also known as the von Mises criterion in the deformation of solids)[1]–[3] to the substrate, we can realize a ~40% reduction of the switching voltage and a consequent ~60% gain in the switching speed. The work highlights the critical role of mechanics and the clamping effect from the substrate in setting the energetics and dynamics of switching in ferroelectrics.

The last three decades have witnessed a significant interest in the science and technology of ferroelectric thin films, driven by the fascinating fundamental physics of the polar state in reduced dimensions as well as the technological applications, for example, in nonvolatile memories[4], [5], which utilize the switchable nature of the ferroelectric polarization to store information. In the case of proper ferroelectrics[6]–[9], where the spontaneous polarization arises from the freezing of a soft-phonon mode at the Curie temperature, the coupling between the dipolar order and the lattice is much stronger than, for example, the coupling of spins to the lattice in ferromagnets[10]–[12]. Focusing on proper ferroelectrics such as $BiFeO_3$ (BFO), $PbTiO_3$ (PTO), and $BaTiO_3$ (BTO) this strong coupling between the lattice and the spontaneous electric dipoles means that switching of the polar state is accompanied by a corresponding, dynamic lattice distortion during switching. With this as background, this work seeks to

answer a question that we believe should be central to the switching of the polar state, namely what is the role of lattice dynamics in influencing ferroelectric switching? For films constrained by a substrate, the clamping effect, or resistance to structural deformation, imposes an additional energy barrier that one must overcome to induce switching. While all thin-film ferroelectrics are subject to constraints imposed by the substrate, clamping effects can play a larger role in inhibiting ferroelastic switching pathways, which are understood to be lower energy for a variety of systems [13], [14] and which are known to be preferred in BFO [15]. This enhanced energy barrier can be understood as a coupling between the dynamic lattice strain and the dipolar order parameter in the system, which manifests itself both in the energy required to switch the state (coercive field) as well as in the switching time (both nucleation and growth regimes of polarization reversal). Further, specific lattice modes (phonons) will also be affected (and potentially stiffened) by the presence of the substrate, which may result in an additional resistance to switching. Understanding both the energetics and dynamics of such coupling, therefore, will provide insight into the limits on ultralow power, high-speed operation of these materials. Such understanding is essential, as the 100 mV switching voltage goal remains a grand challenge for the field[4], [5].

While there have been a large number of studies of quasi-static switching behavior and equilibrium properties of thin films[16]–[20], there have been fewer studies of the limits and timescales of ultrafast switching[21]–[25], and even fewer on the role of lattice dynamics in influencing ferroelectric switching[26]. A key question is how to quantify the role of the substrate in dictating the switching process and whether switching can be studied experimentally without the influence of the substrate. Freestanding ferroelectric membranes have recently emerged as an exciting platform to study the role of mechanical constraints in ferroelectric systems[27], and here, we attempt to quantitatively address the effect of mechanical clamping by using a combination of thermodynamic calculations, phase-field simulations, piezoresponse force microscopy, and

quasi-static and dynamic switching measurements on epitaxial, substrate-attached and freestanding versions of the same thin films (**Fig 1a.**). For our experiments, we use multiferroic BFO, a rhombohedrally distorted perovskite ferroelectric, with a substantial (~5%) lattice distortion because of its large ferroelectric polarization. Further, BFO follows a two-step switching pathway consisting of out-of-plane (109º) and in-plane (71º) steps, thereby, offering an ideal system to study how substrate constraints impact switching. These measurements are also complemented by similar measurements in the literature [26] on thin films of ferroelectric BTO, a prototypical tetragonal ferroelectric, which is used to highlight how substrate clamping impacts a variety of ferroelectric materials. The data reveal a clear impact on the switching voltage (a measure of the barrier energy) as well as the switching dynamics (as manifested by changes in the switching time). Our findings indicate that such effects are broadly applicable to all displacive ferroelectrics.

To quantitatively understand the switching-energy landscape with and without substrate clamping in BFO (**Fig. 1b**), we modeled the thermodynamic free-energy within the context of the Landau theory for ferroelectrics[28]–[30], using a potential of the form

$$f = \alpha_{ij} p_i p_j + \alpha_{ijkl} p_i p_j p_k p_l + \beta_{ij} \theta_i \theta_j + \beta_{ijkl} \theta_i \theta_j \theta_k \theta_l + t_{ijkl} p_i p_j \theta_k \theta_l + \\ + \frac{1}{2} C_{ijkl} (\epsilon_{ij} - \epsilon_{ij}^0)(\epsilon_{kl} - \epsilon_{kl}^0) \quad (1)$$

where p_i, θ_i, and ϵ_{ij} refer to the ferroelectric polarization, ferrodistoritve rotation of the oxygen octahedra, and strain, respectively, while $\epsilon_{ij}^0 = \lambda_{ijkl} \theta_k \theta_l + Q_{ijkl} p_k p_l$. Additional details are provided in Methods and Supporting Information **Section 1, Section 2**. We use two sets of parameters for this Landau potential: a first set directly fitted to first-principles results[31] (nominally at 0 K) and a second one corresponding to the room-temperature Ginzburg-Landau potential for BFO previously introduced in [32], the latter of which is the same model used for the dynamic phase-field simulations of ferroelectric switching discussed below. Guided by previous literature[15], [33], we know that

upon the application of an out-of-plane electric field, BFO typically undergoes 180º switching via a two-step process (**Fig. 1c**): a 109º switch (where the out-of-plane polarization component reverses together with one in-plane component) followed by a 71º switch (where the remaining in-plane component reverses), or *vice versa*. In our thermodynamic analysis, we calculate the free-energy profile associated with the two switching steps while considering different levels of clamping.

First, we calculate the case of no clamping, or the "membrane" case. The energy profiles labeled "membrane" (blue curves in **Fig. 2**) are obtained by continuously varying the transformed polarization components (p_y and p_z for the 109º step, p_x for the 71º switch) while allowing all other variables (remaining polarization components, tilts and strains) to adapt to this change. We observe, as expected[15], [34], that the tilts reverse together with the polarization. This yields the lowest-energy switching paths, corresponding to the experimental case of a free-standing membrane.

Next, to quantify the effect of clamping by the substrate, we perform a set of calculations for various models (*ab initio* and phenomenological) and types of clamping (strain clamping vs. strain + tilt clamping). In order to separate clamping effects from effects of epitaxial misfit strain, we assume the film is thick enough so that it is fully relaxed in its rhombohedral ground state. The fully relaxed nature of the film does not, however, mean that it is free to deform; on the contrary, it is still clamped and, as dictated by the substrate, energetically favors maintaining its original state. We first calculate the energy associated with "strain-clamping" (**Fig. 2a-d**), *i.e.* to obtain the curves labeled "clamped", we impose that strains $\epsilon_{11}, \epsilon_{22}$ and ϵ_{12} be fixed at the values corresponding to the initial state. We obtain similar switching paths the membrane case, with slightly increased energy barriers: about 6% for the 109º step and 20% for the 71º. Notably, the results obtained for the first-principles Landau potential (**Fig. 2a** and **2b**) and the phenomenological model (**Fig. 2c** and **2d**) are essentially equivalent with regards the change in activation energy barriers, highlighting

the efficacy of both methods.

There exist other ways in which the substrate can impact switching, namely by clamping additional order parameters (octahedral tilts) beyond strain. This can arise, for example, by a mismatch in roto-strictive coefficients between the film, electrode and substrate. As such, we show (**Fig. 2e** and **2f**) "strain + tilt clamped" transition paths obtained when all the non-switching polarization and tilt components (as well as $\epsilon_{11}, \epsilon_{22}$ and ϵ_{12}) are held fixed. This immediately results in a greater difference between the membrane and clamped cases (about 64% for both the 109º and 71º steps). In real tri-layer SRO/BFO/SRO films, where the substrate clamping effects and electrode clamping effects are both present, we expect to have a situation that is intermediate between our "strain clamped" and "strain + tilt clamped" cases, which serve as limiting case of clamping effects.

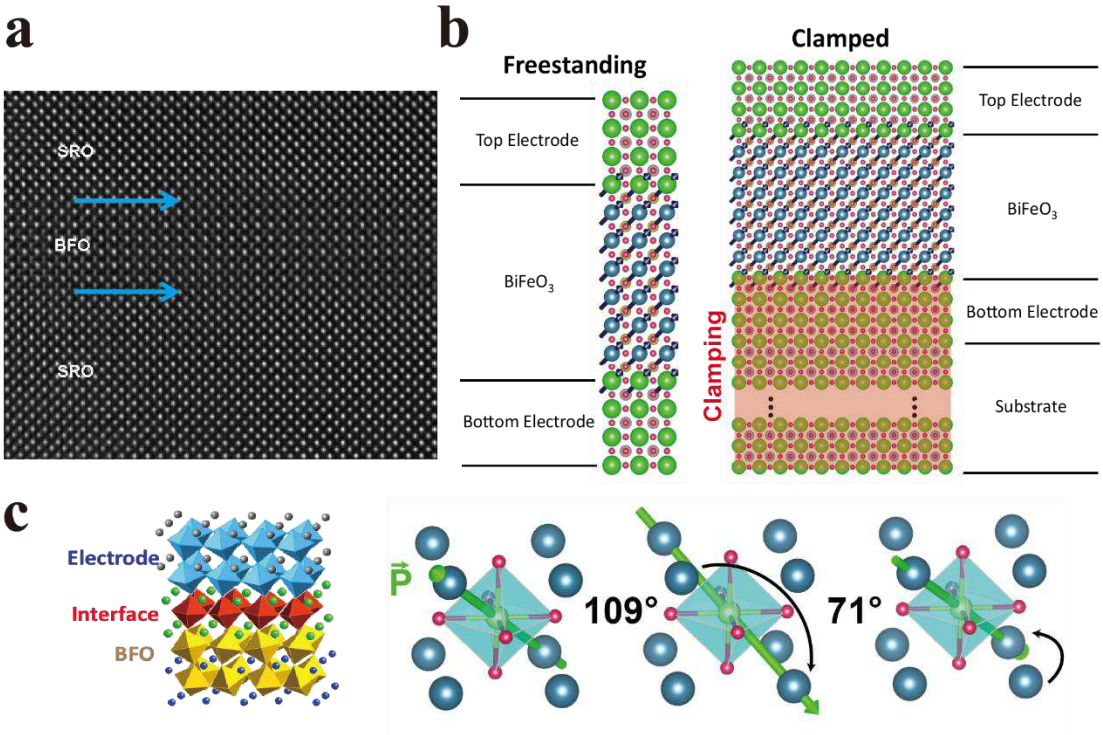

Figure 1. Role of Clamping. a. Transmission electron microscope (TEM) image of SRO/BFO/SRO heterostructure. **b.** Schematic highlighting significant mechanical constraints imposed by the substrate compared with the freestanding film. **c.** SRO/BFO interface schematic showing ferrodistortive oxygen octahedra rotations and switching pathway ($109°$ out-of-plane followed by $71°$in-plane) for BFO films.

To experimentally study the effect of clamping imposed by the substrate,

we employ recent advances in chemically assisted lift-off techniques to produce freestanding BFO layers. Such techniques are rapidly emerging as an approach for tuning the lattice distortion and strain in ferroelectrics[35]–[41]. Several sacrificial layers have been developed, such as water soluble $Sr_3Al_2O_6$[37], acid solution soluble $La_{0.67}Sr_{0.33}MnO_3$ (LSMO)[38], and graphene for mechanical exfoliation[40], leading to freestanding ferroelectric films down to the monolayer limit[27], as well as integration of single-crystalline membranes[40], and flexible layers with super-elasticity[41]. We demonstrate that quantitatively different features are obtained in freestanding BFO membranes versus their clamped counterparts, both in quasistatic measurements of the energetics (coercive field from hysteresis measurements) and dynamical measurements (pulsed switching studies) of the switching process.

Two types of samples were employed for this study. The first type, henceforth referred to as “clamped”, is a Pt (20 nm)/$SrRuO_3$ (SRO 30 nm)/BFO(x nm)/SRO(30 nm), (where x ranges from 12.5 nm to 100 nm) heterostructure (**Fig 1a**) epitaxially grown via pulsed-laser deposition (PLD) on $SrTiO_3$ $(STO)_{[001]}$ substrates (Methods). The second sample type, henceforth referred to as a “membrane”, is a Pt/SRO/BFO/SRO/LSMO stack, that has been subsequently released from the $STO_{[001]}$ substrate by etching the LSMO layer (Supporting Information **Fig. S1**) [38] to completely lift-off the Pt/SRO/BFO/SRO stack from the STO substrate. A supportive PDMS layer is used to then transfer the stack to a Pt/Si (001) substrate. We use an etch rate of ~1 nm/hour to dissolve the LSMO layer in order to avoid deformation or damage of the Pt/SRO/BFO/SRO heterostructure during lift-off. To verify a successful transfer, we measured via atomic force microscopy (AFM) the surface roughness of the initial film and that of the transferred freestanding membrane. Typical measurements are shown (Supporting Information **Fig. S2b** and **S2c**), yielding a surface roughness of 223 pm and 406 pm, respectively, indicating that the high-quality samples can be maintained during this process.

The out-of-plane (*c*) and in-plane (*a*) lattice parameters of the films both before and after lift-off were extracted from X-ray diffraction (XRD) line scans and reciprocal space maps (RSMs). The diffraction results show that the freestanding membranes still possess good epitaxial relationships between BFO and SRO layers (Supporting Information **Fig. S2**). The *c* and *a* lattice-parameter values of the BFO layers calculated from the XRD scans are provided as a function of BFO thickness (**Fig. 3**). We clearly observe that the in-plane lattice constant *a* increases and the out-of-plane lattice constant *c* decreases after the film is released from the substrate. This evolution is succinctly captured by a reduced *c/a* ratio compared to the epitaxial BFO films on substrates. The change in *c/a* for samples with BFO thickness of 8, 35, 60 and 100 nm is in the range of 1.4%-1.9% (**Fig. 3a**), suggesting that the spontaneous distortion, and therefore polarization of BFO membranes is smaller, and the switching-energy barrier between adjacent polarization states should be correspondingly reduced[42]. Notably, the 100-nm-thick BFO clamped film has an in-plane lattice constant (*a* = 3.95 Å) close to its bulk value (*a* = 3.96 Å)[43], indicating the clamped film is nearly completely relaxed and that effects from misfit strain (-1.35% when grown on STO)[44] are minimized at this thickness.

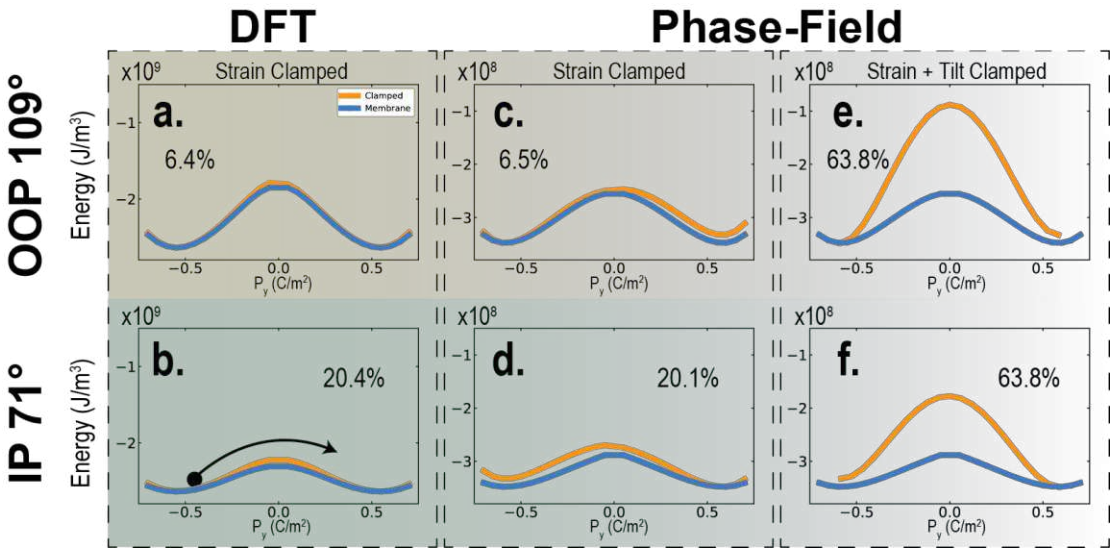

Figure 2. Thermodynamic calculation of switching pathway free energy for BFO. a. and **b.** show 109º (out-of-plane) and 71º (in-plane) switching energy landscapes,

calculated using Landau coefficients obtained from DFT. **c. (d.)** and **e. (f.)** show 109º (71º) double well potentials, respectively, calculated using the Landau potential from the phase-field model in (Supporting Information **Section 1**). In all panels, the "membrane" curves (blue) correspond to a film free of constraints, *i.e.* all order parameters are free to adapt to the switching polarization, which thus corresponds to the lowest-energy transition path. To obtain the "clamped" (orange curves) results in panels **a.** to **d.**, the in-plane strains are held fixed, modeling the effect of strain clamping from the substrate. This results in higher energy barriers, observed. "Clamped" curves in **e.** and **f.** show switching potentials derived from the phase-field model, but with additional constraints imposed; namely, all the non-switching polarization and ferrodistortive (oxygen octahedral tilts) components are held fixed, modeling the limiting case of strain + tilt clamping. Percentages listed are reductions in maximum energy barrier for membrane vs. clamped films in each scenario. Calculations correspond experimentally to the thickest, fully relaxed, films.

The impact of mechanical constraints from the substrate can be observed directly in piezoresponse force microscopy (PFM) imaging of the ferroelectric domain structure before and after release from the substrate. In-plane and out-of-plane PFM amplitude images for both the clamped BFO and freestanding membrane (**Fig 3b,c,** Supporting Information **S3a,b**), reveal dramatic differences. The well-ordered 71° stripe domain pattern of BFO in the clamped film evolves into a "blocky" 180° domain pattern with a larger domain size in the freestanding membrane. These changes are also observed in the corresponding out-plane in-plane and out-plane PFM phase (Supporting Information **Fig. S3c-f**) images for the clamped film and membrane. Kittel's law[45] for ferroelectric domains states that the domain width scales as:

$$w = \sqrt{\frac{\sigma t}{U}} \quad (3)$$

where σ, t, and U are the domain-wall energy, film thickness, and domain energy, respectively. The domain-wall energy is given by:

$$U = U_{dip} + U_x + U_e \quad (4)$$

where U_{dip}, U_x, and U_e are the energy contributions from dipolar interactions (correlation energy), elastic energy, and depolarization energy, respectively[9]. By releasing the film from the substrate, we significantly reduce (or eliminate) the elastic energy (correspondingly leading to an increase in the domain width), and therefore the electrostatic energy becomes the dominant energy scale. In

order to minimize electrostatic energy, ferroelectric domains typically adopt configurations such that $\nabla \cdot P \approx 0$ at domain-wall boundaries, and such a condition is satisfied with 180° domains in perovskite ferroelectrics[9]. We directly observe this effect here, highlighting the dominance of electrostatic energy after removal of elastic constraints. PFM images of BFO samples with thickness of 60, 35, 20 and 8 nm, before and after lift-off are shown (Supporting Information **Fig. S4**). Interestingly, irrespective of the domain structure of the clamped film (*i.e.,* either pure 71° domains or a mixture of 71° and 109° domains), all freestanding membranes feature larger domain sizes and the emergence of an exclusively 180° domain pattern, concomitant with the disappearance of the 71° and 109° domains.

Our experimental PFM results are in good agreement with the mesoscale domain structure modeled by phase-field simulations (using now a complete Ginzburg-Landau potential resolved via the Landau-Khalatnikov dynamical equation[46]). While the 100-nm-thick clamped films (**Fig. 3b)** exhibit two-variant stripe domains, thinner films (Supporting Information **Fig. S4**) exhibit four-variant domain structures. To model the domain structure evolution, we employed phase-field simulations using both four-variant (**Fig. 3d and 3e**) and two-variant initial domain structures (Supporting Information **Fig. S5**). As observed in our simulations, by releasing the film from the substrate, the lateral width of the domain indeed increases dramatically, and 180° domain walls emerge in the freestanding membranes (**Fig. 3e and** Supporting Information **S5c,d**). There are two important considerations in understanding the observed domain structure evolution: misfit strain and the clamping effect from the substrate. By eliminating both via lift-off, the ferroelectric order parameter dominates the Landau free energy, manifesting in the domain structure observed. To disentangle the two effects, and specifically elucidate the role of clamping in the system, we turn to experimental measurements of the energetics and dynamics.

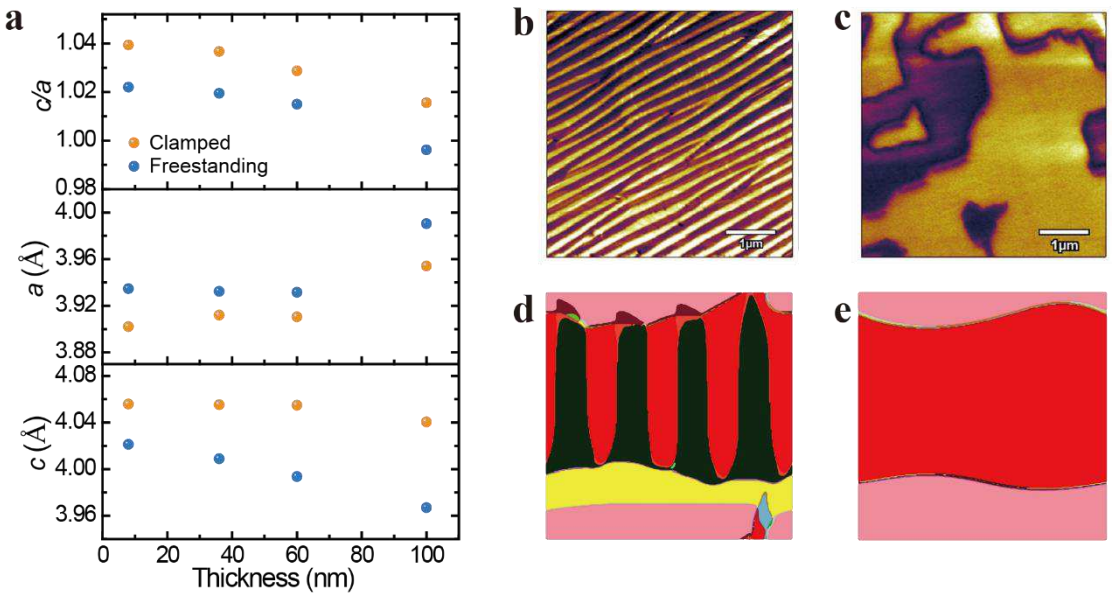

Figure 3. Unit cell distortion of the membranes, and domain structure of the BFO films and freestanding membranes. a, *c, a,* and *c/a* ratio of the BFO films and membranes as a function of thickness. The freestanding BFO membranes exhibit decreased *c*, increased *a*, and decreased *c/a* ratio. **b, c,** In-plane PFM amplitude image of 100-nm BFO film (a) and freestanding membrane (b). **d, e,** Phase-field simulation of BFO layer before (d) and after lift-off (e).

Polarization versus applied voltage (P-V) hysteresis loops on both the clamped films and freestanding membranes were carried out at low temperature (100 K) to minimize the effects of leakage. We compare P-V hysteresis loops measured at 10 kHz for 100-nm and 35-nm BFO clamped films (orange) and membranes (blue), respectively (**Fig 4a** and **Fig 4b**). The data demonstrate that the coercive voltage, defined as the voltage at which the average polarization is zero, measurably decreases upon lift-off. From the hysteresis loops, it is clear that the free-standing membranes also have a lower remnant polarization, consistent with the observed decrease in c/a ratio (**Fig 3a**). Frequency dependent P-V loops were measured (Supporting Information **Fig S6 and Fig S7**) showing less-dispersive, and distinctly lower coercive voltages for the freestanding membranes when compared to the clamped films. Both 100-nm and 35-nm BFO samples show a significant decrease (~40%) in the switching voltage (V_c) after the lift-off process; indeed, this is a general feature of all the thicknesses that we studied (down to at least ~25 nm;

measurements below this thickness were hampered by shorting issues and the mechanical stability of the free-standing membranes below this thickness). The polarization behavior under applied voltage for both clamped and freestanding films was further investigated via PFM-based piezoelectric-hysteresis (both phase and amplitude) loops at room temperature. We can observe a distinct decrease of the switching voltage by ~40% for the samples after lift-off (Supporting Information **Fig. S8**), consistent with our P-V hysteresis loop measurements at low temperature. Notably, the 100-nm-thick clamped film is known to be almost fully relaxed (**Fig 3a**), and since the reductions in switching energy persist even at this film thickness, we conclude that clamping, and resistance to structural distortion *during switching*, plays a dominant role in setting the energetics over effects from misfit strain. The coercive voltage is a measure of the energy required to switch the polarization, and our observed coercive voltage ratios (~40%) between free-standing and clamped films indicate that the clamping effect lies somewhere between strain clamping and strain + tilt clamping (**Fig. 2**). This is an important finding, indicating that it is vital to consider how both strain and oxygen octahedral tilts are affected by clamping.

Having established the role of clamping on switching energetics, we now turn to the dynamics of the switching process. Polarization reversal in ferroelectric thin films is known to proceed via nucleation and growth of reverse polarized domains[18], [21], [47], [48]. We used pulsed ferroelectric measurements[21] to directly measure the ferroelectric polarization evolution during switching. We show polarization transients for various applied voltages for a 25-nm-thick clamped film and freestanding membrane (**Fig. 4c** and Supporting Information **Fig. S9a** and **S9b** show corresponding observed ferroelectric switching displacement current). The saturation polarization of the freestanding membrane is lower than that of the clamped film, consistent with our observed reduction in *c*/*a* ratio (**Fig. 3**) and quasi-static hysteresis loops (**Fig 4a,b**). It is known that RC effects play a significant role in dynamics of

ferroelectric switching in macroscopic device structures at these timescales[21], and as such one must carefully consider differences in resistance stemming from the Pt/Si (001) substrate conductivity after transfer. In order to account for any such effects, we normalized all switching times to the measured RC-time constant for each device (**Fig. 3d**)[21], [26]. Clear decreases in switching time persist even after such normalization verifying that the observed changes are from the mechanical clamping and not changes to extrinsic-circuit parameters. The normalized switching time, defined as the time when the switched polarization reaches 90% of its saturation value, normalized by the non-switching RC-time of the measurement circuit, was extracted for the samples with thicknesses of 25 nm and 60 nm (**Fig. 4d**) with capacitors of the same area. The freestanding membranes show a significant decrease in the switching time compared to the clamped films. Particularly, the 60-nm-thick sample presents a ~63% decrease in the switching time after lift-off. To quantitatively determine the role of clamping from the switching dynamics measurements, we employ Merz' law[48] to extract the ratio of the activation field for the clamped and freestanding films, taking care to account for RC effects in the measurement circuit. Our findings (**Fig. 4d**) shows that the activation voltage for the 25-nm-thick clamped film is 3.45 V while the 25-nm-thick membrane film has an activation voltage of 2.18 V, indicating that the removal of clamping effects results in a $\approx 37\%$ reduction in switching energy. This finding is consistent with the considerable decrease observed in coercive voltage in the hysteresis loops (**Fig 4a,b**) and energy barrier in the thermodynamic calculations (**Fig 2**). Our theoretical predictions (**Fig S10**) are consistent with previous work, which has shown a similar decrease in switching voltage and switching times for BTO freestanding membranes compared to clamped films [26]suggesting a broad applicability of the role of clamping effects in ferroelectric switching.

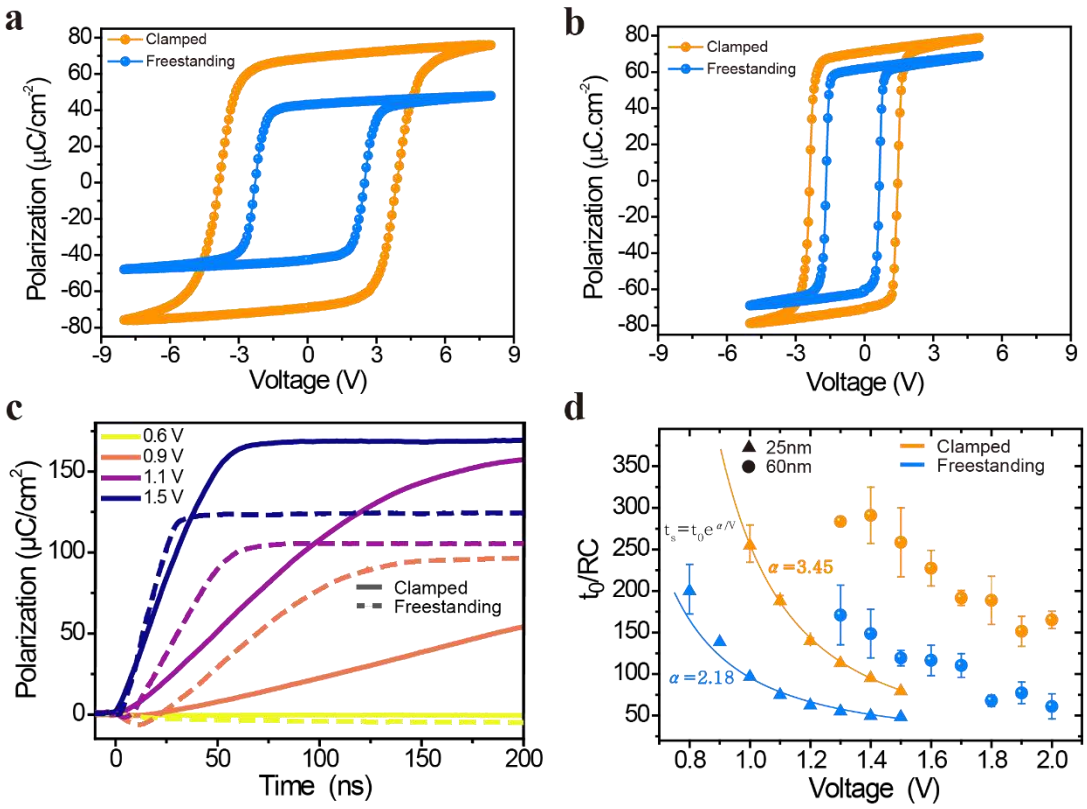

Figure 4. Ferroelectric switching voltage and switching dynamics of BFO films and membranes. Ferroelectric polarization versus voltage (P-V loops) of 100nm (**a**) and 35nm (**b**) clamped films and membranes measured at 10 kHz. **c.** Switching dynamics as a function of applied voltage for the clamped and free-standing films 25nm samples. **d,** Comparison of the extracted switching time (normalized by the RC-time constant) of the samples before (clamped) and after lift-off (freestanding), with BFO thicknesses of 25nm and 60nm. Solid lines and activation voltages (α) are shown for fits to the Merz' law for the 25nm films. These findings show a ~40% reduction in switching energy stemming from substrate clamping effects.

Finally, we performed time-resolved phase-field simulations (Methods, [49]) to further investigate the relevant energy scales and the effects of clamping during switching. We simulated the same applied voltage (13V) for both the clamped and membrane cases, and the evolution of elastic, electric, and Landau energy during the switching process (1000 time steps; where each time step is ~100 fs) were computed[50], [51] (**Fig. 5**). All simulations start from an equilibrium domain state with polarization pointing downwards, a positive voltage is then applied on top to switch the polarization upwards. Changes in the various energy values mean that there are changes in the polarization

distribution within the simulation, with the most dramatic changes occurring as domains are switched. We can clearly see that the time for a freestanding membrane to switch (~20 ps) is significantly shorter than that for the clamped film to switch (~80 ps). Returning now to the fundamental aim of this paper, by examining the time-resolved evolution of the elastic, electric, and Landau energies individually (**Fig 5a-c**), we use our simulations to directly interrogate the role of mechanics during switching. As expected, the elastic energy of the membrane (**Fig. 5a**) is essentially negligible throughout the ferroelectric switching process, except for small local stresses imposed by adjacent domains. The time-resolved elastic energy of the clamped film, on the other hand, remains high, and locally peaks just before switching is completed. These results demonstrate that dynamic evolution of the polar state and accompanying structural distortions transiently modify the energy landscape. Both nucleation and growth of reverse polarized domains are activated processes[48] and both have exponential dependence on the activation energy. As such, even moderate changes in the activation energy can have a dramatic effect on switching time. Furthermore, the elastic energy itself dynamically changes during switching, thereby extending switching timescales. Other energy terms (Landau and electric) are similarly impacted by mechanical constraints, where the high elastic energy slows the evolution of the polarization and results in a higher energy state for longer. The results from these simulations are qualitatively consistent with our experimental results, and quantitatively depict the role of lattice dynamics in ferroelectrics switching. The predicted dynamical speed up from simulation is in good agreement with that observed in experiment (4x vs. ~3-5x). The data presented (**Fig. 5**) includes dynamical evolution of the oxygen octahedral tilts, and as such, an associated energy increase (**Equation 1**). Informed by our earlier findings that the switching energy barrier lies somewhere between strain clamping and strain + tilt clamping, and to extract the effect on switching from the octahedral tilts, we simulate the same polarization switching (**Fig. S11**) without oxygen octahedral

tilts. There is a stark contrast between these two cases, with the oxygen octahedral tilts accounting for a ~10x increase in switching time over the case where oxygen octahedral tilts are not considered. This is a novel finding, and the dramatic increase in switching time highlights the importance of proper consideration of all coupled order parameters in setting the dynamics and energetics of switching in BFO.

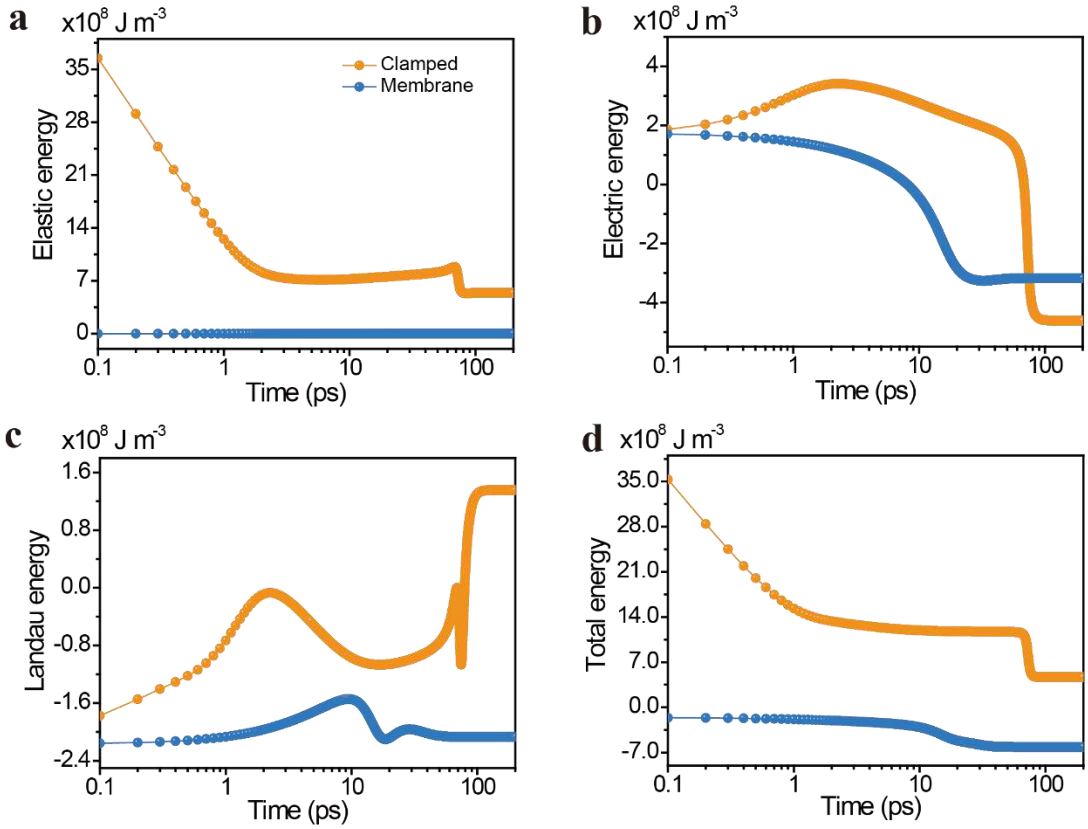

Figure 5. Free energy evolution during the switching process under an externally applied voltage for clamped film and membrane cases. Horizontal axis is the time in picosecond (ps) and vertical axis is the average energy of the corresponding component within the whole simulation system in J cm^{-3}. **(a)** Elastic energy. **(b)** Electrostatic energy. **(c)** Landau energy. **(d)** Total free energy which is the summation of the elastic electrostatic, and Landau energy. For the clamped film case, 0.4% compressive mismatch strain is considered.

In conclusion, our work reveals the fundamental role of mechanical constraints in ferroelectric switching in BFO, and more broadly, for displacive ferroelectric thin film materials in general. With the grand challenge of achieving sub-100mV switching in ferroelectrics, clamping effects and the relative

contribution to switching energetics and dynamics of all coupled order parameters much be understood. We employ a Landau free energy formalism to conduct thermodynamic calculations modeling the clamping effect from the substrate, both using *ab-initio* and phenomenological models. We experimentally demonstrate a method of mitigating clamping effects by lifting-off SRO/BFO/SRO trilayers from an STO substrate. Other methods, for example, by tuning device aspect ratio[52] may provide additional pathways to mitigate clamping. Here, we observe a marked evolution of crystal and domain structure, consistent with changes in elastic constraints. This study shows that the energetics and dynamics of the system, drastically change after lift-off, and we observe a significant reduction in switching voltage and improved switching speeds for freestanding membranes relative to clamped films. The origins of the changes observed are better understood with the help of phase-field simulations, where the dynamic elastic energy and oxygen octahedral tilts play a predominant role in delaying polarization reversal.

Acknowledgements

The work at Berkeley is supported by ASCENT, one of the six SRC-JUMP centers. Support from Intel Corporation under the FEINMAN Program (E.P.) is also gratefully acknowledged. A.F. acknowledges support from the Army Research Office under Grant W911NF-21-1-0118. Q.W. acknowledges support from Teacher Training Funds of Sichuan University. D.P. acknowledges support from the European Union's Horizon 2020 research and innovation program under the Marie Skłodowska-Curie grant agreement No. 79712 and from the National Science Foundation under grant Grant DMR-1708615 for work done at Berkeley. L.W.M. and R.R. acknowledge support from the Army Research Office under the ETHOS MURI via cooperative agreement W911NF-21-2-0162. N.F and J.Í. acknowledge support from the Semiconductor Research Corporation and Intel, via contract no. 2018-IN-2865. X.C. and L.-Q.C. acknowledges supports from the U.S. Department of Energy, office of Science, Basic Energy Sciences, under award no. DE-SC0020145. R.-C. P. acknowledges supports from the Natural Science Foundation of China (grant no. 51902247) and Natural Science Foundation of Shanxi Province (grant no. 2020JQ-059).

Methods

Film growth. The oxide heterostructures BFO/SRO/LSMO or SRO/BFO/SRO/LSMO were grown on single-crystalline (001) STO substrate by pulsed laser deposition at 650-720 ℃ with focused laser fluence ~1.2 J cm^{-2} in 100-160 mTorr oxygen pressure and cooled down to room temperature in 400 Torr oxygen pressure. To protect the film during the lift-off process, a 20-nm Pt layer was deposited on top of the SRO or BFO layer by magnetron sputtering. The top SRO layer was patterned into circular top electrode and the bottom SRO layer served as a bottom electrode for ferroelectric switching testing.

Lift-off process. PDMS stamps were cut into 8 mm x 8 mm x 1.5 mm from a commercial specimen (Gelfilm from Gelpal). Then they were stacked tightly onto the film. After floating the PDMS/films in an etching solution (low-concentration HCl solution (0.3 vol %) mixed with 0.1 mol mL^{-1} potassium iodide) for several hours, the LSMO dissolved to lift the freestanding film off STO substrate, which were washed with deionized water and dried with N_2 gas. The samples were then moved onto Si/Pt substrate. The entire stack was annealed at 110 ℃ for 30 min to promote adhesion at the film/new substrate interface. After cooling to 70 ℃ and peeling off the PDMS stamp with tweezers, the transferred membrane on Si/Pt substrate was obtained.

X-ray diffraction (XRD) and reciprocal space mapping (RSM). The films before and after freestanding were measured with a Panalytical Empyrean diffractometer (Cu-$K\alpha_1$, 1.540598 Å), using a hybrid, two-bounce primary monochromator on the incident beam. RSM of the samples were acquired with the same incident beam optics and a PIXcel^{3D} position-sensitive detector, using the frame-based 1D mode with a step time of 10 s.

Piezoresponse force microscopy (PFM). PFM was performed with an Atomic Force Microscope (Asylum Research Cypher, Santa Barbara, CA), conductive AFM probe (Nanoandmore, DT-NCHR, Watsonville, CA) with the DART mode. The typical contact resonance frequency is 260 kHz and its higher harmonics.

Polarization testing. For polarization switching measurements (P-V loops), we used the patterned circular top electrodes with diameter of 16 μm at the frequency of 1 Hz-100 kHz at both room temperature and 100 K with Precision Multiferroic tester (Radiant Technologies).

Phase-field simulation. The current phase-field model for ferroelectric free standing film is an extension to our previous model for bulk and epitaxial thin film simulations[30], [32], [51], [53], in which we use the spontaneous polarization ***P***=(*P*1, *P*2, *P*3) and oxygen octahedral tilt $\theta = (\theta_1, \theta_2, \theta_3)$ as the order parameter to represent the ferroelectric domain structure evolution that is couple to the elastic and electric state of the whole system. A temporal evolution of the order parameter spatial distribution can be obtained by solving the time-dependent Ginzburg-Landau equation:

$\frac{\partial P_i(\mathbf{r},t)}{\partial t} = -L\frac{\delta F_{\mathrm{tot}}}{\delta P_i(\mathbf{r},t)}$, (*i*=1, 2, 3)

$\frac{\partial \theta_i(\mathbf{r},t)}{\partial t} = -L\frac{\delta F_{\mathrm{tot}}}{\delta \theta_i(\mathbf{r},t)}$, (*i*=1, 2, 3)

In which *L* is the kinetic coefficient related to the domain wall mobility, *t* is time, and **r** is the spatial coordinate, $F_{tot}$is the total free energy of BFO membrane, given as,

$F_{\mathrm{tot}} = \iiint_{V_{BFO}}(f_{land} + f_{grad} + f_{elec} + f_{elast})dV$, and $f_{Land} = \alpha_{ij}p_ip_j + \alpha_{ijkl}p_ip_jp_kp_l + \beta_{ij}\theta_i\theta_j + \beta_{ijkl}\theta_i\theta_j\theta_k\theta_l + t_{ijkl}p_ip_j\theta_k\theta_l$ represent the local free energy densities of Landau energy, which includes the landan energy for polarization, oxygen octahedral tilt and the coupling terms, $f_{grad} = \frac{1}{2}g_{ijkl}p_{i,j}p_{k,l} + \kappa_{ijkl}\theta_{i,j}\theta_{k,l}$represents the gradient energy, which includes the gradient energy for both polarization and oxygen octahedral tilt, $f_{elect} =$

$-\frac{1}{2}\mathrm{E_i p_i}$ represents the electrostatic energy, and $f_{elastic} = \frac{1}{2}C_{ijkl}(\varepsilon_{ij} - \varepsilon_{ij}^0)(\varepsilon_{kl} - \varepsilon_{kl}^0)$represents the elastic energy, in which the eigenstrain is determined by the order parameters $\varepsilon_{ij}^0 = \lambda_{ijkl}\theta_k\theta_l + Q_{ijkl}p_k p_l$. There are two differences between the current free-standing film and our previous epitaxial thin film model[32], all of which are in the elastic part. First, for the free-standing film, both the top and bottom surface are set as traction-free boundaries, as shown in equation (2) owing to the nature of the freestanding membrane,

$$\begin{cases} \sigma_{i3}|_{z=1} = 0 \\ \sigma_{i3}|_{z=h_f} = 0, \end{cases} \quad \text{(i=1,2,3)} \quad (2)$$

where h_f means the membrane thickness. Second, since overall free-standing film is in a stress-free state, the in-plane macroscopic strain is set to be the average eigenstrain calculated from the current order parameter distribution. All physical parameters in the above equations are listed in the Supporting Information.

References

[1] Z. F. Zhang and J. Eckert, “Unified Tensile Fracture Criterion,” *Phys. Rev. Lett.*, vol. 94, no. 9, p. 094301, Mar. 2005, doi: 10.1103/PhysRevLett.94.094301.

[2] T. H. Courtney, *Mechanical Behavior of Materials*, 2nd edition. Long Grove, Illinois: Waveland Pr Inc, 2005.

[3] R. Hill, *The Mathematical Theory of Plasticity*, 2nd edition. Oxford : New York: Oxford University Press, 1998.

[4] G. W. Burr, B. N. Kurdi, J. C. Scott, C. H. Lam, K. Gopalakrishnan, and R. S. Shenoy, “Overview of candidate device technologies for storage-class memory,” *IBM J. Res. Dev.*, vol. 52, no. 4.5, pp. 449–464, Jul. 2008, doi: 10.1147/rd.524.0449.

[5] S. Manipatruni *et al.*, “Scalable energy-efficient magnetoelectric spin–orbit logic,” *Nature*, vol. 565, no. 7737, pp. 35–42, Jan. 2019, doi: 10.1038/s41586-018-0770-2.

[6] K. F. Garrity, K. M. Rabe, and D. Vanderbilt, “Hyperferroelectrics: Proper Ferroelectrics with Persistent Polarization,” *Phys. Rev. Lett.*, vol. 112, no. 12, p. 127601, Mar. 2014, doi: 10.1103/PhysRevLett.112.127601.

[7] E. Bousquet *et al.*, “Improper ferroelectricity in perovskite oxide artificial superlattices,” *Nature*, vol. 452, no. 7188, pp. 732–736, Apr. 2008, doi: 10.1038/nature06817.

[8] K. A. Müller and H. Burkard, “SrTi${\mathrm{O}}_{3}$: An intrinsic quantum paraelectric below 4 K,” *Phys. Rev. B*, vol. 19, no. 7, pp. 3593–3602, Apr. 1979, doi: 10.1103/PhysRevB.19.3593.

[9] M. E. Lines and A. M. Glass, *Principles and Applications of Ferroelectrics and Related Materials*. Oxford: Oxford University Press, 2001. doi: 10.1093/acprof:oso/9780198507789.001.0001.

[10] S. Chikazumi, *Physics of Ferromagnetism*. Oxford, New York: Oxford University Press, 1997.

[11] A. H. Morrish, *The Physical Principles of Magnetism*, 1st edition. New York: Wiley-IEEE Press, 2001.

[12] H. I. Seo, S. Woo, J. Kim, S. G. Jeong, T. Park, and W. S. Choi, “Crystalline symmetry-dependent magnon formation in the itinerant ferromagnet $\mathrm{SrRu}{\mathrm{O}}_{3}$,” *Phys. Rev. B*, vol. 103, no. 4, p. 045104, Jan. 2021, doi: 10.1103/PhysRevB.103.045104.

[13] R. Xu *et al.*, “Kinetic control of tunable multi-state switching in ferroelectric thin films,” *Nat. Commun.*, vol. 10, no. 1, p. 1282, Mar. 2019, doi: 10.1038/s41467-019-09207-9.

[14] R. Xu *et al.*, “Ferroelectric polarization reversal via successive ferroelastic transitions,” *Nat. Mater.*, vol. 14, no. 1, pp. 79–86, Jan. 2015, doi: 10.1038/nmat4119.

[15] J. T. Heron *et al.*, “Deterministic switching of ferromagnetism at room temperature using an electric field,” *Nature*, vol. 516, no. 7531, pp. 370–373, Dec. 2014, doi: 10.1038/nature14004.

[16] J. Y. Jo *et al.*, “Polarization Switching Dynamics Governed by the Thermodynamic Nucleation Process in Ultrathin Ferroelectric Films,” *Phys. Rev. Lett.*, vol. 97, no. 24, p. 247602, Dec. 2006, doi: 10.1103/PhysRevLett.97.247602.

[17] J. Y. Jo, H. S. Han, J.-G. Yoon, T. K. Song, S.-H. Kim, and T. W. Noh, “Domain Switching Kinetics in Disordered Ferroelectric Thin Films,” *Phys. Rev. Lett.*, vol. 99, no. 26, p. 267602, Dec. 2007, doi: 10.1103/PhysRevLett.99.267602.

[18] Y. Ishibashi and Y. Takagi, “Note on Ferroelectric Domain Switching,” *J. Phys. Soc. Jpn.*, vol. 31, no. 2, pp. 506–510, Aug. 1971, doi: 10.1143/JPSJ.31.506.

[19] H. Chang *et al.*, “Watching domains grow: In-situ studies of polarization switching by

combined scanning probe and scanning transmission electron microscopy," *J. Appl. Phys.*, vol. 110, no. 5, p. 052014, Sep. 2011, doi: 10.1063/1.3623779.

[20] C. Alessandri, P. Pandey, A. Abusleme, and A. Seabaugh, "Switching Dynamics of Ferroelectric Zr-Doped HfO2," *IEEE Electron Device Lett.*, vol. 39, no. 11, pp. 1780–1783, Nov. 2018, doi: 10.1109/LED.2018.2872124.

[21] E. Parsonnet *et al.*, "Toward Intrinsic Ferroelectric Switching in Multiferroic ${\mathrm{BiFeO}}_{3}$," *Phys. Rev. Lett.*, vol. 125, no. 6, p. 067601, Aug. 2020, doi: 10.1103/PhysRevLett.125.067601.

[22] A. Grigoriev, M. M. Azad, and J. McCampbell, "Ultrafast electrical measurements of polarization dynamics in ferroelectric thin-film capacitors," *Rev. Sci. Instrum.*, vol. 82, no. 12, p. 124704, Dec. 2011, doi: 10.1063/1.3665209.

[23] P. K. Larsen, G. L. M. Kampschöer, M. J. E. Ulenaers, G. a. C. M. Spierings, and R. Cuppens, "Nanosecond switching of thin ferroelectric films," *Appl. Phys. Lett.*, vol. 59, no. 5, pp. 611–613, Jul. 1991, doi: 10.1063/1.105402.

[24] M. Si *et al.*, "Ultrafast measurements of polarization switching dynamics on ferroelectric and anti-ferroelectric hafnium zirconium oxide," *Appl. Phys. Lett.*, vol. 115, no. 7, p. 072107, Aug. 2019, doi: 10.1063/1.5098786.

[25] S. Bhattacharjee, D. Rahmedov, D. Wang, J. Íñiguez, and L. Bellaiche, "Ultrafast Switching of the Electric Polarization and Magnetic Chirality in ${\mathrm{BiFeO}}_{3}$ by an Electric Field," *Phys. Rev. Lett.*, vol. 112, no. 14, p. 147601, Apr. 2014, doi: 10.1103/PhysRevLett.112.147601.

[26] D. Pesquera *et al.*, "Beyond Substrates: Strain Engineering of Ferroelectric Membranes," *Adv. Mater.*, vol. 32, no. 43, p. 2003780, 2020, doi: 10.1002/adma.202003780.

[27] D. Ji *et al.*, "Freestanding crystalline oxide perovskites down to the monolayer limit," *Nature*, vol. 570, no. 7759, pp. 87–90, Jun. 2019, doi: 10.1038/s41586-019-1255-7.

[28] W. L. Zhong, Y. G. Wang, P. L. Zhang, and B. D. Qu, "Phenomenological study of the size effect on phase transitions in ferroelectric particles," *Phys. Rev. B*, vol. 50, no. 2, pp. 698–703, Jul. 1994, doi: 10.1103/PhysRevB.50.698.

[29] N. A. Pertsev, A. G. Zembilgotov, and A. K. Tagantsev, "Effect of Mechanical Boundary Conditions on Phase Diagrams of Epitaxial Ferroelectric Thin Films," *Phys. Rev. Lett.*, vol. 80, no. 9, pp. 1988–1991, Mar. 1998, doi: 10.1103/PhysRevLett.80.1988.

[30] Y. L. Li, S. Y. Hu, Z. K. Liu, and L. Q. Chen, "Effect of substrate constraint on the stability and evolution of ferroelectric domain structures in thin films," *Acta Mater.*, vol. 50, no. 2, pp. 395–411, Jan. 2002, doi: 10.1016/S1359-6454(01)00360-3.

[31] N. Fedorova, D. Nikonov, I. Young, and J. Íñiguez, *Prep.*, 2021.

[32] F. Xue, Y. Gu, L. Liang, Y. Wang, and L.-Q. Chen, "Orientations of low-energy domain walls in perovskites with oxygen octahedral tilts," *Phys. Rev. B*, vol. 90, no. 22, p. 220101, Dec. 2014, doi: 10.1103/PhysRevB.90.220101.

[33] S. H. Baek *et al.*, "Ferroelastic switching for nanoscale non-volatile magnetoelectric devices," *Nat. Mater.*, vol. 9, no. 4, pp. 309–314, Apr. 2010, doi: 10.1038/nmat2703.

[34] J. X. Zhang *et al.*, "Microscopic Origin of the Giant Ferroelectric Polarization in Tetragonal-like ${\mathrm{BiFeO}}_{3}$," *Phys. Rev. Lett.*, vol. 107, no. 14, p. 147602, Sep. 2011, doi: 10.1103/PhysRevLett.107.147602.

[35] S. R. Bakaul *et al.*, "Ferroelectric Domain Wall Motion in Freestanding Single-Crystal Complex

Oxide Thin Film," *Adv. Mater.*, vol. 32, no. 4, p. 1907036, 2020, doi: 10.1002/adma.201907036.

[36] D. Lu, D. J. Baek, S. S. Hong, L. F. Kourkoutis, Y. Hikita, and H. Y. Hwang, "Synthesis of freestanding single-crystal perovskite films and heterostructures by etching of sacrificial water-soluble layers," *Nat. Mater.*, vol. 15, no. 12, pp. 1255–1260, Dec. 2016, doi: 10.1038/nmat4749.

[37] S. S. Hong *et al.*, "Two-dimensional limit of crystalline order in perovskite membrane films," *Sci. Adv.*, vol. 3, no. 11, p. eaao5173, Nov. 2017, doi: 10.1126/sciadv.aao5173.

[38] D. Pesquera *et al.*, "Large magnetoelectric coupling in multiferroic oxide heterostructures assembled via epitaxial lift-off," *Nat. Commun.*, vol. 11, no. 1, p. 3190, Jun. 2020, doi: 10.1038/s41467-020-16942-x.

[39] G. Dong *et al.*, "Super-elastic ferroelectric single-crystal membrane with continuous electric dipole rotation," *Science*, vol. 366, no. 6464, pp. 475–479, Oct. 2019, doi: 10.1126/science.aay7221.

[40] H. S. Kum *et al.*, "Heterogeneous integration of single-crystalline complex-oxide membranes," *Nature*, vol. 578, no. 7793, pp. 75–81, Feb. 2020, doi: 10.1038/s41586-020-1939-z.

[41] R. Guo *et al.*, "Continuously controllable photoconductance in freestanding BiFeO 3 by the macroscopic flexoelectric effect," *Nat. Commun.*, vol. 11, no. 1, p. 2571, May 2020, doi: 10.1038/s41467-020-16465-5.

[42] Y.-L. Huang *et al.*, "Manipulating magnetoelectric energy landscape in multiferroics," *Nat. Commun.*, vol. 11, no. 1, p. 2836, Jun. 2020, doi: 10.1038/s41467-020-16727-2.

[43] S. Li and T. Birol, "Suppressing the ferroelectric switching barrier in hybrid improper ferroelectrics," *Npj Comput. Mater.*, vol. 6, no. 1, pp. 1–10, Nov. 2020, doi: 10.1038/s41524-020-00436-x.

[44] A. Haykal *et al.*, "Antiferromagnetic textures in BiFeO3 controlled by strain and electric field," *Nat. Commun.*, vol. 11, p. 1704, Apr. 2020, doi: 10.1038/s41467-020-15501-8.

[45] C. Kittel, "Theory of the Structure of Ferromagnetic Domains in Films and Small Particles," *Phys. Rev.*, vol. 70, no. 11–12, pp. 965–971, Dec. 1946, doi: 10.1103/PhysRev.70.965.

[46] Y.-C. Liao *et al.*, "Simulation of the Magnetization Dynamics of a Single-Domain $BiFeO_3$ Nanoisland," *IEEE Trans. Magn.*, vol. 56, no. 10, pp. 1–9, Oct. 2020, doi: 10.1109/TMAG.2020.3011932.

[47] Y.-H. Shin, I. Grinberg, I.-W. Chen, and A. M. Rappe, "Nucleation and growth mechanism of ferroelectric domain-wall motion," *Nature*, vol. 449, no. 7164, pp. 881–884, Oct. 2007, doi: 10.1038/nature06165.

[48] W. J. Merz, "Domain Formation and Domain Wall Motions in Ferroelectric BaTi${\mathrm{O}}_{3}$ Single Crystals," *Phys. Rev.*, vol. 95, no. 3, pp. 690–698, Aug. 1954, doi: 10.1103/PhysRev.95.690.

[49] A. R. Damodaran *et al.*, "Phase coexistence and electric-field control of toroidal order in oxide superlattices," *Nat. Mater.*, vol. 16, no. 10, pp. 1003–1009, Oct. 2017, doi: 10.1038/nmat4951.

[50] B. Winchester, N. Balke, X. X. Cheng, A. N. Morozovska, S. Kalinin, and L. Q. Chen, "Electroelastic fields in artificially created vortex cores in epitaxial BiFeO3 thin films," *Appl. Phys. Lett.*, vol. 107, no. 5, p. 052903, Aug. 2015, doi: 10.1063/1.4927750.

[51] F.-Y. Lin, X. Cheng, L.-Q. Chen, and S. B. Sinnott, "Strain effects on domain structures in

ferroelectric thin films from phase-field simulations," *J. Am. Ceram. Soc.*, vol. 101, no. 10, pp. 4783–4790, 2018, doi: 10.1111/jace.15705.

[52] V. Nagarajan *et al.*, "Dynamics of ferroelastic domains in ferroelectric thin films," *Nat. Mater.*, vol. 2, no. 1, pp. 43–47, Jan. 2003, doi: 10.1038/nmat800.

[53] R.-C. Peng *et al.*, "Understanding and predicting geometrical constraint ferroelectric charged domain walls in a BiFeO3 island via phase-field simulations," *Appl. Phys. Lett.*, vol. 113, no. 22, p. 222902, Nov. 2018, doi: 10.1063/1.5050802.

Supplementary Files

This is a list of supplementary files associated with this preprint. Click to download.

- SupplementaryinformationforTheroleoflatticedynamicsinferroelectricswitching.pdf